Journal of Alloys and Compounds 821 (2020) 153499

Contents lists available at ScienceDirect

Journal of Alloys and Compounds

journal homepage: http://www.elsevier.com/locate/jalcom

Reduction in thermal conductivity of Sb_2Te phase-change material by scandium/yttrium doping

Liyu Peng [a, b], Zhen Li [a, b], Guanjie Wang [a, b], Jian Zhou [a, b], Riccardo Mazzarello [c], Zhimei Sun [a, b, *]

[a] School of Materials Science and Engineering, Beihang University, Beijing, 100191, China
[b] Center for Integrated Computational Materials Science, International Research Institute for Multidisciplinary Science, Beihang University, Beijing, 100191, China
[c] Institute for Theoretical Solid State Physics, RWTH Aachen University, Aachen, 52074, Germany

ARTICLE INFO

Article history:
Received 23 September 2019
Received in revised form
18 December 2019
Accepted 21 December 2019
Available online 26 December 2019

Keywords:
Phase change material
Sc-doped
And Y-doped Sb_2Te
Thermal conductivity

ABSTRACT

Binary Sb_2Te is considered as a potential recording material for phase-change memory due to its higher crystallization speed than the widely investigated ternary Ge-Sb-Te alloys. To further improve the performance of Sb_2Te, various dopants such as scandium (Sc) have been explored. Yet, the thermal conductivity of the pristine and doped Sb_2Te is unknown, even though the thermal conductivity (κ) is an essential parameter for phase change memory devices as thermal conductivity determines the exchange of energy with surroundings and heat transport in the SET/RESET process. In this work, by means of *ab initio* calculations, we have calculated the thermal conductivity of Sb_2Te, scandium (Sc)-doped and yttrium (Y)-doped Sb_2Te. The calculated lattice thermal conductivity values at 300 K are 3.76 $Wm^{-1}K^{-1}$, 3.22 $Wm^{-1}K^{-1}$ and 3.35 $Wm^{-1}K^{-1}$ for pristine Sb_2Te, Sc-doped Sb_2Te, and Y-doped Sb_2Te, respectively, showing a reduction in lattice thermal conductivity by doping. Further analysis of the electron localization function and Bader charge distribution suggest that the increased bonding strength of the dopants with the surrounding atoms contributes to the reduction in lattice thermal conductivity of the doped Sb_2Te. On the other hand, the electronic thermal conductivity of Sb_2Te should also decrease due to the metal to semiconductor transition by Sc/Y doping as analyzed by the calculated density of states. Overall, the thermal conductivity of Sb_2Te decreases to some extent by doping Sc and Y, which can lower the energy consumption and improve the efficiency of energy utilization in the data SET/RESET process and is thus desirable for phase-change memory devices.

1. Introduction

The ever increasing development of the information technologies has put a high priority on the density, stability, and speed of the nonvolatile memories. The mainstream technology utilizing Flash memory now is reaching its dimension limit [1], which motivates researchers to search for new materials with different storage mechanism. The most promising candidates are the phase-change materials (PCMs) [2,3] for phase-change random access memory (PCRAM), which utilize the rapid and reversible phase transitions between crystalline and amorphous states of PCMs to record the information, while the large resistance difference between the two states is used to read the stored data. Herein, the phase change speed from the amorphous to crystalline state (also called SET operation) or, in other words, the crystallization speed limits the speed of PCRAM devices. The outstanding properties, such as low costs, high scalability and high integration level [4] of PCRAMs have made them promising candidates for nonvolatile memories. Some PCRAM products have already been commercialized. The performance of PCRAM highly depends on the properties of phase-change materials. The most popular PCMs are the Ge-Sb-Te (GST) alloys along the Sb_2Te_3-GeTe pseudo-binary compositional tie-line. Numerous works have been devoted to understanding their fundamental properties including structure [5,6], phase change mechanism [7], as well as improving their overall performance by searching for proper dopants [8–10]. Nevertheless, the relatively long SET time that is around 50ns for $Ge_2Sb_2Te_5$ [11] hinders the

* Corresponding author. School of Materials Science and Engineering, Beihang University, Beijing, 100191, China.
E-mail address: zmsun@buaa.edu.cn (Z. Sun).

https://doi.org/10.1016/j.jallcom.2019.153499
0925-8388/

large-scale commercial applications of PCRAM. Thus searching for new materials with short SET time is key to making high-speed PCRAM devices. Among the explored new PCRAM, binary Sb_2Te has attracted great attention due to its high crystallization speed with a short SET time of around 6 ns [12], which benefits from its growth-dominated crystallization process in sharp contrast to the nucleation-dominated process of ternary GST alloys. Meanwhile, various dopants, for example, Y [8], Sc [12], Ti [13], Ag and In [14,15], Cr [16], Zn [17], C [18], N [19], have been explored to improve the thermal stability of Sb_2Te and hence the data retention ability of its PCRAM.

Thermal conductivity is a fundamental property of phase change materials and hence PCRAM. There is a significant energy exchange between the material and its surroundings in the SET/RESET process. As a result, a low conductivity means a low thermal dissipation and a high efficiency of energy utilization and thus it plays an important role in the dynamic process of the reversible transformation. Yet the thermal conductivity of the pristine and doped Sb_2Te have not been explored. Therefore, it is essential to investigate the thermal conductivity of Sb_2Te and its doped system as the corresponding data is unknown so far. In this work, by means of *ab initio* calculations, we have calculated the thermal conductivity of pristine and Sc/Y doped Sb_2Te alloys. Our results show that the lattice thermal conductivity of Sb_2Te is 3.76 $Wm^{-1}K^{-1}$ at 300 K, which is rather high and is undesirable for PCRAM, while it reduces to 3.22 $Wm^{-1}K^{-1}$ and 3.35 $Wm^{-1}K^{-1}$ for Sc-doped and Y-doped Sb_2Te, respectively. Then, the underlying mechanism responsible for the reduction is explored by the electron localization function and Bader charge distribution analysis. Finally, we show that the Sc/Y doping also results in the reduction in the electronic thermal conductivity of Sb_2Te due to the metal to semiconductor transition induced by doping. Overall, the reduction in thermal conductivity of Sb_2Te due to Sc or Y doping is beneficial to improve the efficiency of energy utilization and hence the power consumption of PCRAM devices.

2. Computational methods

Our calculations were carried out within the framework of density-functional theory (DFT) as implemented in the Vienna *ab initio* simulation package (VASP) [20]. The projector-augmented wave (PAW) potentials [21] were used with the generalized-gradient approximation (GGA) [22] and the Perdew-Burke-Ernzerhof (PBE) exchange-correlation functional [23]. The cut-off energy for the plane-wave expansion of the Kohn-Sham states was tested to be 300 eV for convergence. The convergence criterion for the total energy was set as less than 1×10^{-5} eV. A *k*-point mesh of $7 \times 7 \times 1$ was automatically generated with their origin at the Γ point, and the tetrahedron method with Blöchl corrections [24] was used. The *k*-point grid has been proved to be sufficient to obtain converged results. To better describe the effects of the nonbonding interactions, a semi-empirical dispersion potential was added to the conventional Kohn-Sham DFT energy in the scheme of the DFT-D2 method [6,25] for all structure optimization calculations. The optimized lattice constants a and c are 4.29 Å and 17.77 Å, which are in good agreement with the experimental results [26]. Moreover, as the GGA potentials always underestimate the band gap size, we used the Heyd-Scuseria-Ernzerhof (HSE06) hybrid functional [27] with accurate exchange and correlation energy to calculate the band gaps. For calculations of the mechanical properties and lattice thermal conductivity, we used the structure with the nominal formula of $ScSb_5Te_3$, YSb_5Te_3 for Sc doped, Y doped Sb_2Te respectively. Finally, the *ab initio* molecular dynamics (AIMD) simulations in the NVT ensemble with a Nosè-Hoover thermostat at a temperature of 400 K were used for the evaluation of the dynamic stability and the mean square displacement (MSD). For AIMD simulations, the ensemble of $4 \times 4 \times 1$ Sb_2Te hexagonal supercell containing 144 atoms was annealed at 400K for 30 ps, where a time step of 3 fs was adopted.

3. Results and discussion

3.1. Structure of doped Sb_2Te

As illustrated in Fig. 1(a), Sb_2Te (space group **P$\bar{3}$m1**) consists of Sb bilayers (denoted as BLs) and Sb_2Te_3 quintuple layers (denoted as QLs) [28], resulting in periodically repeated nine layers Te1−Sb1−Te2−Sb2−Sb3−Sb3−Sb2−Te2−Sb1 stacked along the c axis. The vdW interactions exist between the adjacent BLs and QLs, and the adjacent BLs [28]. A unit cell with nine atoms containing six Sb atoms and three Te atoms was used to calculate the formation energy in this work. There are five possible substitutional sites of Sb1, Sb2, Sb3, Te1, Te2 for the dopants. The interstitial sites between BLs are too narrow to accommodate the doped elements. Therefore, we only considered the interstitial (denoted as *i*) between QLs and 2BLs. The formation energies for doping Sc and Y at these six sites have been calculated using the equation (1):

$$E_f[X] = E_{tot}[X] - E_{tot}[bulk] - \sum_i n_i \mu_i \quad (1)$$

Where $E_{tot}[X]$, $E_{tot}[bulk]$ are the total energies of the unit cell with and without Sc and Y dopant respectively, and n_i indicates the number of atoms of type *i* (host atoms or doped atoms) that have been added to ($n_i > 0$) or removed from ($n_i < 0$) the unit cell when Sc or Y is doped in Sb_2Te, and μ_i is the corresponding chemical potential of these elements, which depends on the experimental growth condition. Under the extreme condition of Te-rich, the upper limit of chemical potential of Te is subject to the relation: $\mu_{Te}^{max} = \mu_{Te}[bulk]$. Similarly, under the extreme condition of Te-poor, the lower limit of the chemical potential of Te can be deduced as: $\mu_{Te}^{min} = (E_{tot}(Sb_2Te) - 6\mu_{Sb}[bulk])/3$. The bulk chemical potentials of Sb, Te, Sc, and Y are calculated with the corresponding unit cell respectively from ICSD [29] (Inorganic Crystal Structure Database).

The calculated formation energies are shown in Fig. 1(d). It is seen that substituting for Sb1 is the most favorable both for Sc-doped Sb_2Te (denoted as Sc−Sb_2Te) and Y-doped Sb_2Te (denoted as Y−Sb_2Te) as the formation energies are the lowest compared with other cases. Hence we can conclude that the doped Y or Sc atoms occupy in an octahedral environment with sixfold coordination, similar to other dopants, e.g., Al [30]. The electro-negativity difference (ΔS) of Sc (1.36)-Te (2.12), Y (1.22)-Te (2.12) are much larger than that of Sb (2.05)-Te (2.12), and a larger ΔS means a higher nucleation rate that will give rise to a smaller grain size distribution after doping with Sc, Y which have been confirmed by experiments [12]. The stability of Sc/Y-doped Sb_2Te has been also checked (see Supplemental Material). To characterize the stability of the Sb_2Te, Sc−Sb_2Te, and Y−Sb_2Te, we have performed *ab initio* molecular dynamics simulations (AIMD) to check the structure evolution with time, where a temperature of 400 K was chosen as this is roughly the temperature for the test of 10-years data retention for PCRAM. The good dynamic stability of Sc−Sb_2Te and Y−Sb_2Te is seen by the total energy evolution with time for the doped materials system (see the Supplemental Material).

3.2. Mechanical properties and lattice thermal conductivity

For Sb_2Te, Sc−Sb_2Te, Y−Sb_2Te, which belong to the trigonal crystal system, there are six independent elastic stiffness constant c_{11}, c_{12}, c_{13}, c_{14}, c_{33}, c_{44} with the following forms [6,31]:

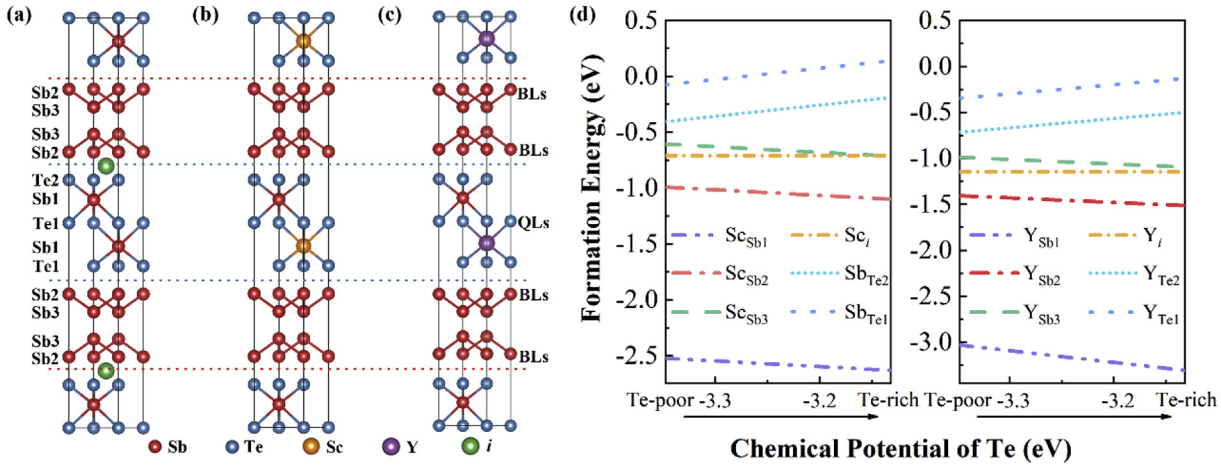

Fig. 1. The 1 × 1 × 2 supercells of (a) Sb_2Te, (b) Sc substituting Sb1, (c) Y substituting Sb1. Each slab is formed by two Sb bilayers (BLs) and Sb_2Te_3 quintuple layers (QLs). There are five possible substitutional sites at Sb1, Sb2, Sb3, Te1, Te2, and an interstitial site *i* between the adjacent Te2 and Sb2. (d) The formation energy of that Sc, Y atom occupy six places of Sb1, Sb2, Sb3, Te1, Te2, interstitial site (denoted as *i*).

$$\begin{bmatrix} c_{11} & c_{12} & c_{13} & c_{14} & 0 & 0 \\ c_{12} & c_{11} & c_{13} & -c_{14} & 0 & 0 \\ c_{13} & c_{13} & c_{33} & 0 & 0 & 0 \\ c_{14} & -c_{14} & 0 & c_{44} & 0 & 0 \\ 0 & 0 & 0 & 0 & c_{44} & c_{14} \\ 0 & 0 & 0 & 0 & c_{14} & c_{66} \end{bmatrix} \quad (2)$$

The elastic constants are obtained by determining the Hessian matrix, i.e., the matrix of the second derivatives of the energy with respect to the atomic positions. According to the Voigt-Reuss-Hill approximation [32], the bulk modulus (B) and the shear modulus (G) can be evaluated by calculating the elastic modulus of the trigonal crystal structures. It is well known that the Voigt bound based on the uniform strain corresponds to the upper limit of the actual modulus, while the Reuss bound from the uniform stress is the lower limit. The two bounds agree with each other as seen in Table 1. Based on the bulk modulus B_H calculated from the Hill approximation with the sequence of Sb_2Te > Sc−Sb_2Te > Y−Sb_2Te, it is concluded that the resistance to compression of Sb_2Te decreases after doping Sc and Y. According to Pugh's principle [33] for predicting the ductility of a material, the order of B/G (Sc−Sb_2Te > Y−Sb_2Te) indicates that Sc−Sb_2Te will exhibit a better ductility than Y−Sb_2Te.

Based on the above-calculated bulk and shear moduli, we use Navier's equation [37] to get the longitudinal elastic wave velocity υ_l and the transverse elastic wave velocity υ_s as well as the mean sound velocity υ_m (see the supplemental material). Then, the Debye temperature θ_D which characterizes the total vibrational spectrum is estimated by the following Eq. (3) as given by Clarke [38]:

$$\theta_D = \frac{h}{k_B}\left[\frac{3n}{4\pi}\left(\frac{\rho N_A}{M}\right)\right]^{1/3} \upsilon_m \quad (3)$$

where h is the Planck constant, k_B is the Boltzmann constant, N_A is the Avogadro number, M is the molecular weight.

The Grüneisen constant γ characterizes the high-order anharmonic term, which is of great importance for the property of thermal conductivity. More specifically, the Grüneisen constant γ is a measure of the deviation of a crystal from harmonicity [39]. It is defined as $\gamma = -\frac{d\ln\omega_i}{d\ln V}$ where ω_i is the vibration frequency of a given module with volume V. It can be derived from Poisson's ratio (ν) that can be derived from the bulk modulus (B) and the shear modulus (G) as follows:

$$\nu = \frac{3B - 2G}{2(3B + G)} \quad (4)$$

$$\gamma = \frac{3}{2}\left(\frac{1+\nu}{2-3\nu}\right) \quad (5)$$

The calculated density ρ (g/cm^3), mean sound velocity υ_m (km/s), Debye temperature θ_D, Grüneisen constant γ are listed in Table 2. Generally, low elastic properties such as Young's modulus and shear modulus mean a weak chemical bonding stiffness in materials, which will usually soften phonon mode and slow down phonon propagation [40]. The order of the calculated mean sound velocity υ_m in Y−Sb_2Te > Sc−Sb_2Te > Sb_2Te corresponds to that of B_H.

The thermal conductivity in a semiconductor can be separated into two distinct parts: the electron thermal conductivity and the

Table 2
The calculated density ρ (g/cm^3), mean sound velocity υ_m (km/s), Grüneisen constant γ, and the Debye temperature θ_D.

System	ρ (g/cm^3)	υ_m (Km/s)	γ	θ_D (K)
Sb_2Te	6.65	2.08	1.40	197.14
Sc−Sb_2Te	6.21	2.03	1.42	192.77
Y−Sb_2Te	6.27	2.02	1.40	190.16

Table 1
The calculated elastic constants c_{ij} (Gpa), bulk modulus (B), shear modulus (G) of Sb_2Te and Sc−Sb_2Te, Y−Sb_2Te. B_V, G_V is calculated from the Voigt approximation [34], and B_R, G_R is from the Reuss bound [35], and the Hill approximation [36] is used to obtain the B_H, G_H (see the supplemental material).

Gpa	c_{11}	c_{12}	c_{13}	c_{14}	c_{33}	c_{44}	B_V	G_V	G_R	G_R	B_H	G_H
Sb_2Te	85.88	23.63	23.65	21.25	35.22	35.54	38.76	29.51	32.09	17.32	35.42	23.42
Sc−Sb_2Te	80.80	23.83	22.37	12.78	28.47	27.08	36.35	24.63	27.43	17.06	31.89	20.84
Y−Sb_2Te	78.29	21.37	21.29	14.54	29.95	27.75	34.94	24.96	27.94	16.94	31.44	20.95

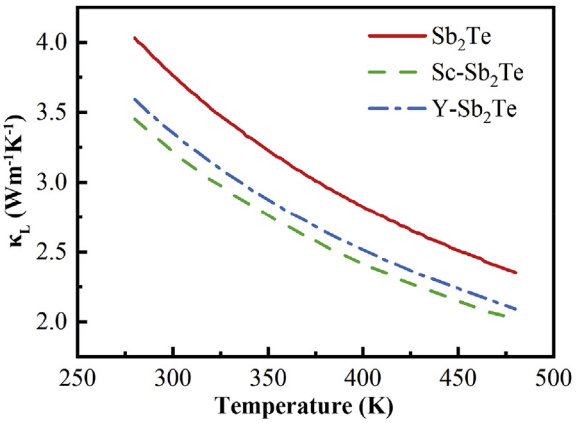

Fig. 2. The absolute temperature-dependent lattice thermal conductivity of Sb_2Te, Sc−Sb_2Te, and Y−Sb_2Te. (Sc/Y−Sb_2Te refers to the configuration in which Sc/Y atoms substitute for the Sb1 atoms).

lattice thermal conductivity contributed by lattice vibration in the form of longitudinal and transverse elastic waves. Considering that acoustic modes play an essential role in the heat transfer and the main form of phonon interactions in the heat-conduction process was via Umklapp process, Slack [39] provided an equation to obtain the lattice thermal conductivity which depends on the temperature:

$$\kappa_L = A(\gamma) \cdot \frac{M\theta_D^3\delta}{\gamma^2 n^{2/3} T} (T \geq \theta) \quad (6)$$

Where $A(\gamma) = 2.43 \times 10^7/(1 - 0.514/\gamma + 0.228/\gamma^2)$, $\overline{M}$ [kg/mol] is the mean atomic mass, δ^3 [m^3] is the average volume of one atom in the primitive unit cell, θ_D [K] is the Debye temperature, T [K] is the absolute temperature, γ is the Grüneisen constant.

Finally, we can get the relationship between the lattice thermal conductivity and the absolute temperature of Sb_2Te, Sc−Sb_2Te, Y−Sb_2Te as shown in Fig. 2. It is seen that the lattice thermal conductivity for the three materials decreases drastically with temperature which is attributed to the increased anharmonicity via the enhanced umklapp process. At 300 K, the lattice thermal conductivity for Sb_2Te, Sc−Sb_2Te, and Y−Sb_2Te are estimated to be 3.76 $Wm^{-1}K^{-1}$, 3.22 $Wm^{-1}K^{-1}$, and 3.35 $Wm^{-1}K^{-1}$, respectively, showing a significant decrease in lattice thermal conductivity due to doping. The value (3.76 $Wm^{-1}K^{-1}$) of lattice thermal conductivity at 300 K of the undoped Sb_2Te is comparable to the total thermal conductivity (~8 $Wm^{-1}K^{-1}$) measured by Masashi KUWAHARA et al. [41], where a thin-film sample of thickness 1 μm was used in the nanosecond thermoreflectance measurement. It is expected as the pure Sb_2Te presents a metallic character, which will be shown below, and will therefore have an additional electronic contribution of the thermal conductivity. It is worth mentioning that Sb/Te compositional disorder [14] which could be pronounced upon fast crystallization should also decrease the lattice thermal conductivity.

To understand the underlying mechanism of the reduction in lattice thermal conductivity of the doped system, the mean square displacement (MSD) averaged over atoms, $\langle \Delta R^2 \rangle(t)$, is estimated for Sc−$Sb_2Te$ and Y−Sb_2Te as seen from Fig. 3(a) and (b) respectively. Note that Sb and Te vibrate around a constant value of ~0.12 $Å^2$ away from their initial configurations as a function of simulation time, while the doped atoms, Sc and Y, vibrate around that of ~0.1 $Å^2$. Typically, the MSD of a lightweight atom should be higher than the MSD of a heavy atom. However, both the mean square displacement of Sc and Y in Fig. 3 are lower than that of the pristine atoms. Hence, we further studied the underlying causes of this phenomenon through electron localization function (ELF) analysis and Bader charge analysis.

The interactions between dopants and pristine atoms could be visualized through the electron localization functions (ELF) analyses projected on the (110) plane, as illustrated in Fig. 4. The dark colors between the centers of Sb1 and Te2 in Sb_2Te indicate the densely localized electrons that is indicative of strong covalent bonds, while the chemical bonding between the dopants and Te is more ionic.

To quantitatively characterize the amount of the charge transfer in Sc−Sb_2Te and Y−Sb_2Te, the Bader charge [42] has been calculated, which is depicted in Fig. 5. Note that the average accepted electrons by Te in Sc−Sb_2Te (0.71) and Y−Sb_2Te (0.76) increases compared with Sb_2Te (0.36) due to the charge transfer from the doping elements to Te. Furthermore, the results of the wave-function-based Mullilken charge [43] analysis also coincides with the Bader charge analysis (see the Supplemental Material). As a result, the bond between the doping element and Te tends to be ionic like that of Ag in Sb_2Te [44]. Consequently, the stronger bond strength after doping leads to the lower MSD of the lightweight atoms, and thus the decrease of lattice thermal conductivity.

3.3. The density of states and electronic thermal conductivity

As for the electronic thermal conductivity k_e, it obeys the law of

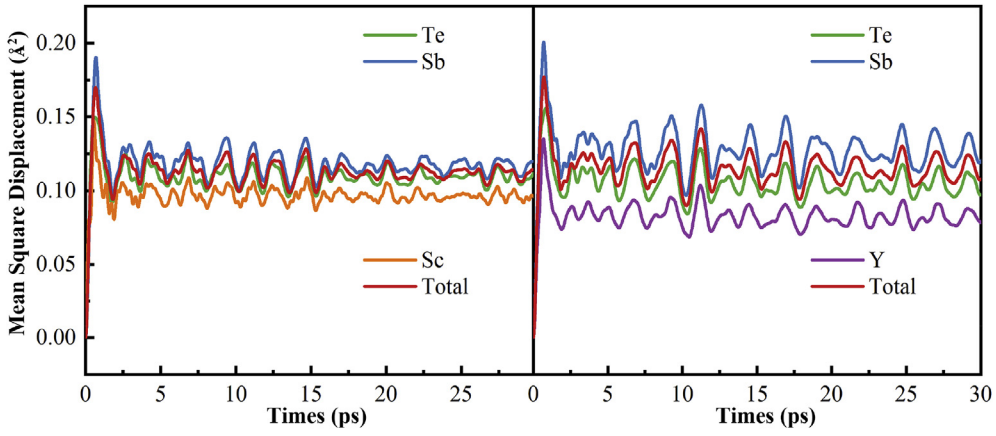

Fig. 3. The mean square displacements of (a) Sc−Sb_2Te, and (b) Y−Sb_2Te. (Sc/Y−Sb_2Te refers to the configuration in which Sc/Y atoms substitute for the Sb1 atoms).

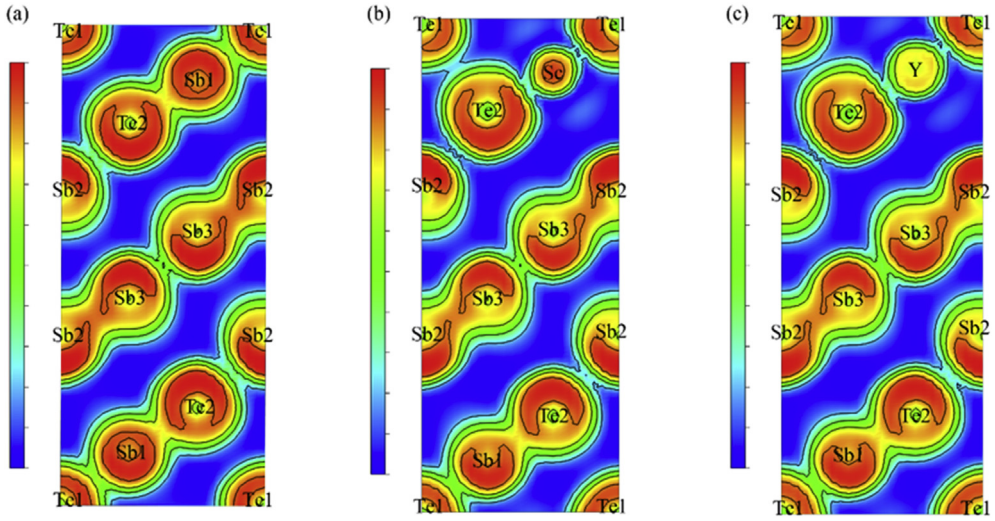

Fig. 4. The electron localization function (ELF) of (a) Sb_2Te, (b) Sc−Sb_2Te, and (c) Y−Sb_2Te. (Sc/Y−Sb_2Te refers to the configuration in which Sc/Y atoms substitute for the Sb1 atoms).

Widemann-Franz: $\kappa_e = L\sigma T$, where L is the Lorenz constant and σ is the electronic conductivity including the contributions of both electron and hole carriers. Note that the electronic thermal conductivity κ_e is inversely proportional to the effective mass m*, and m* increases with the energy gap E_g according to the $k\cdot p$ perturbation theory [45], which yields the following relation:

$$\frac{m}{m^*} \approx \frac{2\sum_{\nu}|\langle c|p|\nu\rangle|^2}{mE_g}. \tag{7}$$

As clearly seen in Fig. 6, both of Sc−Sb_2Te and Y−Sb_2Te are semiconductor with $E_g = 0.159$ eV and 0.316 eV respectively while Sb_2Te shows a metallic character. This implies that the electronic thermal conductivities should significantly decrease after doping Sc and Y. The conduction band edge of the doped Sb_2Te is mainly contributed by the Sb 5p orbit and the Sc/Y p orbit. Compared with the pristine Sb_2Te, the conduction bands of doped Sb_2Te system shift upward and thus results in a metal-to-semiconductor transition. The increase in the gap energy may be attributed to the increased ionic character and their stronger bonding after doping. Furthermore, the electronic thermal conductivity can be ignored at room temperature as in other cases, e.g., Y doped Sb_2Te_3 [31]. So it is reasonable to conclude that the thermal conductivities are reduced after doping with Sc or Y. This reduction is especially crucial for decreasing heat dissipation and transport in the SET/RESET process for applications of PCM in the non-volatile memory. The reduction in the thermal conductivity can decrease the thermal cross-talk between adjacent memory cells and thus can facilitate size down-scaling in phase-change memory devices. On the other hand, it is also beneficial to reduce the heating current needed for switching, and thereby decreases the power consumption.

4. Conclusions

In summary, by performing *ab initio* calculations, it is found that Sc or Y dopants prefer to substitute the Sb1 atoms and the bond between the doping element and Te tends to be ionic. Our results show that Sc/Y can lower the lattice thermal conductivity, which can be attributed to the stronger ionic bonds between the Sc/Y and pristine atoms according to the electron localization function (ELF) analysis and the Bader charge analysis. Furthermore, the doping elements can also open an electronic gap, which decreases the electronic thermal conductivity, and the ability of data retention and the amorphous stability are proved to be enhanced after doping [12]. The reduced thermal conductivity is expected to facilitate the improvement of energy efficiency and the increase in memory storage density. Our results are helpful to better optimize the performance of Sb_2Te-based phase change random access memory (PCRAM) devices, especially in the application of the high-speed phase change materials (DRAM).

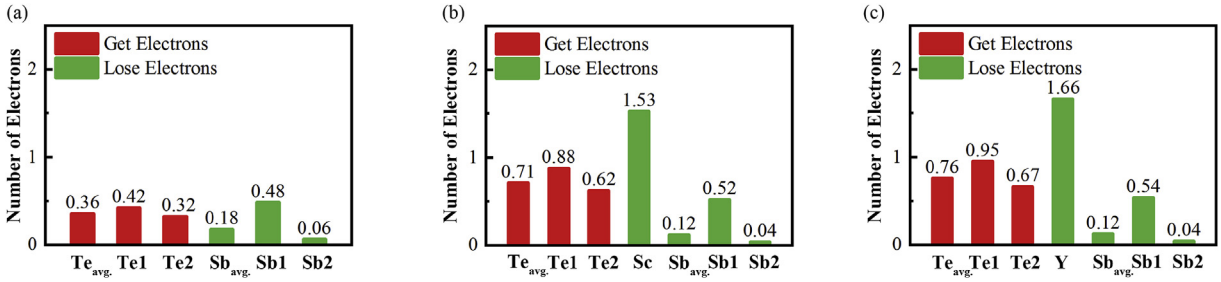

Fig. 5. The Bader Charge of (a) Sb_2Te, (b) Sc−Sb_2Te, and (c) Y−Sb_2Te. (Sc/Y−Sb_2Te refers to the configuration in which Sc/Y atoms substitute for the Sb1 atoms) The red bars represent the acquisition of electrons, and the green bars represent the loss of electrons. The $Te_{avg.}$ and $Sb_{avg.}$ mean the number of electrons averaged on Te and Sb respectively. (For interpretation of the references to color in this figure legend, the reader is referred to the Web version of this article.)

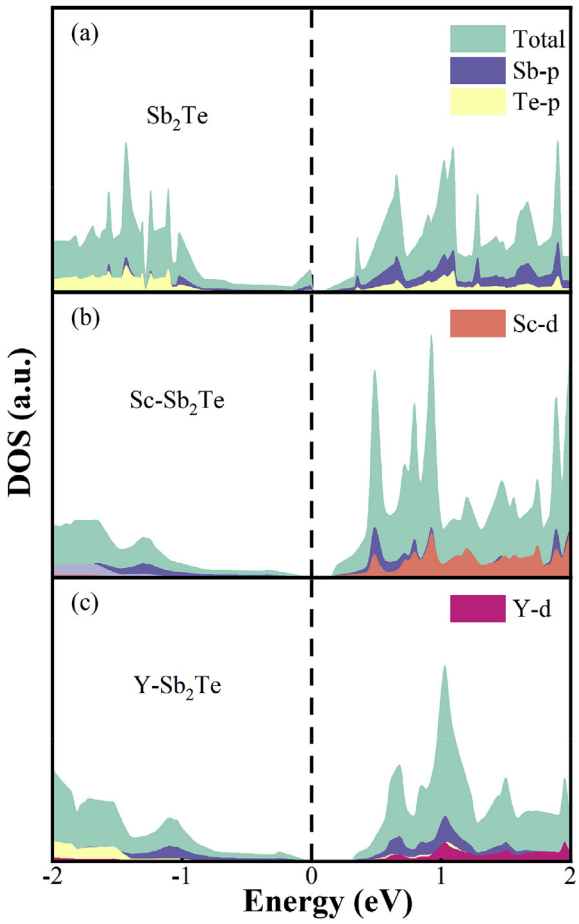

Fig. 6. The density of states (DOS) of (a) Sb_2Te, (b)Sc−Sb_2Te, and (c)Y−Sb_2Te. (Sc/Y−Sb_2Te refers to the configuration in which Sc/Y atoms substitute for the Sb1 atoms).

Credit author statement

Liyu Peng: Investigation, Methodology, Formal Analysis, Data Curation, Validation, Writing-original draft, Writing-review & editing.

Zhen Li: Investigation, Formal Analysis, Validation.

Guanjie Wang: Investigation, Software, Validation.

Jian Zhou: Conceptualization, Supervision, Project administration, Writing-Review & Editing.

Riccardo Mazzarello: Writing-review & editing.

Zhimei Sun: Conceptualization, Supervision, Funding acquisition, Resources, Project administration, Writing-review & editing.

Declaration of competing interest

The authors declare that they have no known competing financial interests or personal relationships that could have appeared to influence the work reported in this paper.

Acknowledgements

This work is financially supported by the National Key Research and Development Program of China (Grant No. 2017YFB0701700), the National Natural Science Foundation of China (Grant No. 51872017) and the 111 Project (B17002).

Appendix A. Supplementary data

Supplementary data to this article can be found online at https://doi.org/10.1016/j.jallcom.2019.153499.

References

[1] C.-Y. Lu, K.-Y. Hsieh, R. Liu, Future challenges of flash memory technologies, Microelectron. Eng. 86 (2009) 283–286.
[2] M. Wuttig, Towards a universal memory? Nat. Mater. 4 (2005) 265.
[3] W. Zhang, R. Mazzarello, M. Wuttig, E. Ma, Designing crystallization in phase-change materials for universal memory and neuro-inspired computing, Nat. Rev. Mater. 4 (2019) 150–168.
[4] G.W. Burr, M.J. Breitwisch, M. Franceschini, D. Garetto, K. Gopalakrishnan, B. Jackson, B. Kurdi, C. Lam, L.A. Lastras, A. Padilla, B. Rajendran, S. Raoux, R.S. Shenoy, Phase change memory technology, Journal of Vacuum Science & Technology B, Nanotechnology and Microelectronics: Materials, Processing, Measurement, and Phenomena 28 (2010) 223–262.
[5] Z. Sun, J. Zhou, R. Ahuja, Structure of phase change materials for data storage, Phys. Rev. Lett. 96 (2006), 055507.
[6] B. Sa, J. Zhou, R. Ahuja, Z. Sun, First-principles investigations of electronic and mechanical properties for stable $Ge_2Sb_2Te_5$ with van der Waals corrections, Comput. Mater. Sci. 82 (2014) 66–69.
[7] Z. Sun, J. Zhou, Y. Pan, Z. Song, H.K. Mao, R. Ahuja, Pressure-induced reversible amorphization and an amorphous-amorphous transition in $Ge_2Sb_2Te_5$ phase-change memory material, Proc. Natl. Acad. Sci. U. S. A. 108 (2011) 10410–10414.
[8] Z. Li, C. Si, J. Zhou, H. Xu, Z. Sun, Yttrium-doped Sb_2Te_3: a promising material for phase-change memory, ACS Appl. Mater. Interfaces 8 (2016) 26126–26134.
[9] G. Wang, J. Zhou, S.R. Elliott, Z. Sun, Role of carbon-rings in polycrystalline $GeSb_2Te_4$ phase-change material, J. Alloy. Comp. 782 (2019) 852–858.
[10] L. Zhang, S. Song, W. Xi, L. Li, Z. Song, Effect of Ti additions on structure and phase stability of Sb_2Te_3 thin films by experimental and theoretical methods, J. Mater. Sci. Mater. Electron. 29 (2017) 4704–4710.
[11] I.S. Kim, S.L. Cho, D.H. Im, E.H. Cho, D.H. Kim, G.H. Oh, D.H. Ahn, S.O. Park, S.W. Nam, J.T. Moon, C.H. Chung, High performance PRAM cell scalable to sub-20nm technology with below $4F^2$ cell size, extendable to DRAM applications, in: 2010 Symposium on VLSI Technology, 2010, pp. 203–204.
[12] X. Chen, Y.H. Zheng, M. Zhu, K. Ren, Y. Wang, T. Li, G.Y. Liu, T.Q. Guo, L. Wu, X.Q. Liu, Y. Cheng, Z.T. Song, Scandium doping brings speed improvement in Sb_2Te alloy for phase change random access memory application, Sci. Rep. 8 (2018).
[13] M. Zhu, L. Wu, Z. Song, F. Rao, D. Cai, C. Peng, X. Zhou, K. Ren, S. Song, B. liu, S. Feng, $Ti_{10}Sb_{60}Te_{30}$ for phase change memory with high-temperature data retention and rapid crystallization speed, Appl. Phys. Lett. 100 (2012).
[14] W. Zhang, I. Ronneberger, P. Zalden, M. Xu, M. Salinga, M. Wuttig, R. Mazzarello, How fragility makes phase-change data storage robust: insights from ab initio simulations, Sci. Rep. 4 (2014) 6529.
[15] T. Matsunaga, J. Akola, S. Kohara, T. Honma, K. Kobayashi, E. Ikenaga, R.O. Jones, N. Yamada, M. Takata, R. Kojima, From local structure to nano-second recrystallization dynamics in AgInSbTe phase-change materials, Nat. Mater. 10 (2011) 129–134.
[16] M.H. Jiang, Q. Wang, Y. Wang, B. Liu, Y. Meng, S. Wen, J.S. Wei, Z.T. Song, Y.Q. Wu, Optical properties of Cr-doped Sb_2Te thin films during ultrafast crystallization processes, J. Non-Cryst. Solids 469 (2017) 56–61.
[17] X. Shen, G.X. Wang, R.P. Wang, S.X. Dai, L.C. Wu, Y.M. Chen, T.F. Xu, Q.H. Nie, Enhanced thermal stability and electrical behavior of Zn-doped Sb_2Te films for phase change memory application, Appl. Phys. Lett. 102 (2013).
[18] G.X. Wang, X. Shena, Q.H. Nie, H. Wang, Y.G. Lu, D.T. Shi, Improved thermal stability of C-doped Sb_2Te films by increasing degree of disorder for memory application, Thin Solid Films 615 (2016) 345–350.
[19] M. Zhu, L.C. Wu, F. Rao, Z.T. Song, X.L. Li, C. Peng, X.L. Zhou, K. Ren, D.N. Yao, S.L. Feng, N-doped Sb_2Te phase change materials for higher data retention, J. Alloy. Comp. 509 (2011) 10105–10109.
[20] G. Kresse, J. Hafner, Ab initio molecular dynamics for open-shell transition metals, Phys. Rev. B 48 (1993) 13115–13118.
[21] P.E. Blöchl, Projector augmented-wave method, Phys. Rev. B 50 (1994) 17953–17979.
[22] J.P. Perdew, K. Burke, M. Ernzerhof, Generalized gradient approximation made simple, Phys. Rev. Lett. 77 (1996) 3865–3868.
[23] J.P. Perdew, Y. Wang, Accurate and simple analytic representation of the electron-gas correlation energy, Phys. Rev. B 45 (1992) 13244–13249.
[24] P.E. Blöchl, O. Jepsen, O.K. Andersen, Improved tetrahedron method for Brillouin-zone integrations, Phys. Rev. B 49 (1994) 16223–16233.
[25] S. Grimme, Semiempirical GGA-type density functional constructed with a long-range dispersion correction, J. Comput. Chem. 27 (2006) 1787–1799.
[26] V. Agafonov, N. Rodier, R. Ceolin, R. Bellissent, C. Bergman, J.P. Gaspard, Structure of Sb_2Te, Acta Crystallogr. C 47 (1991) 1141–1143.
[27] J. Heyd, G.E. Scuseria, M. Ernzerhof, Hybrid functionals based on a screened Coulomb potential, J. Chem. Phys. 118 (2003) 8207–8215.
[28] L. Khalil, E. Papalazarou, M. Caputo, N. Nilforoushan, L. Perfetti, A. Taleb-Ibrahimi, V. Kandyba, A. Barinov, Q.D. Gibson, R.J. Cava, M. Marsi, Electronic

band structure for occupied and unoccupied states of the natural topological superlattice phase Sb_2Te, Phys. Rev. B (2017) 95.
[29] A. Belsky, M. Hellenbrandt, V.L. Karen, P. Luksch, New developments in the Inorganic Crystal Structure Database (ICSD): accessibility in support of materials research and design, Acta Crystallogr. B 58 (2002) 364–369.
[30] Y. Wang, T. Wang, Y. Zheng, G. Liu, T. Li, S. Lv, W. Song, S. Song, Y. Cheng, K. Ren, Z. Song, Atomic scale insight into the effects of Aluminum doped Sb_2Te for phase change memory application, Sci. Rep. 8 (2018) 15136.
[31] Z. Li, N. Miao, J. Zhou, H. Xu, Z. Sun, Reduction of thermal conductivity in $Y_xSb_{2-x}Te_3$ for phase change memory, J. Appl. Phys. 122 (2017) 195107.
[32] J.M.J.d. Toonder, J.A.W.v. Dommelen, F.P.T. Baaijens, The relation between single crystal elasticity and the effective elastic behaviour of polycrystalline materials: theory, measurement and computation, Model. Simul. Mater. Sci. Eng. 7 (1999) 909.
[33] S.F. Pugh, XCII. Relations between the elastic moduli and the plastic properties of polycrystalline pure metals, The London, Edinburgh, and Dublin Philosophical Magazine and Journal of Science 45 (2009) 823–843.
[34] W. Voigt, Lehrbuch der kristallphysik (mit ausschluss der kristalloptik), Springer-Verlag, 2014.
[35] A. Reuss, Stresses constant in composite, rule of mixtures for compliance components, J. Appl. Math. Mech. 9 (1929) 49–58.
[36] R. Hill, The elastic behaviour of a crystalline aggregate, Proc. Phys. Soc. Sect. A 65 (1952) 349.
[37] O. Anderson, E. Schreiber, N. Soga, Elastic Constants and Their Measurements, McGraw-Hill, New York, 1973.
[38] D.R. Clarke, Materials selection guidelines for low thermal conductivity thermal barrier coatings, Surf. Coat. Technol. 163 (2003) 67–74.
[39] D.T. Morelli, G.A. Slack, High lattice thermal conductivity solids, in: S.L. Shindé, J.S. Goela (Eds.), High Thermal Conductivity Materials, Springer New York, New York, NY, 2006, pp. 37–68.
[40] Y. Xiao, C. Chang, Y. Pei, D. Wu, K. Peng, X. Zhou, S. Gong, J. He, Y. Zhang, Z. Zeng, L.-D. Zhao, Origin of low thermal conductivity in SnSe, Phys. Rev. B (2016) 94.
[41] M. Kuwahara, O. Suzuki, N. Taketoshi, T. Yagi, P. Fons, J. Tominaga, T. Baba, Thermal conductivity measurements of Sb–Te alloy thin films using a nanosecond thermoreflectance measurement system, Jpn. J. Appl. Phys. 46 (2007) 6863–6864.
[42] G. Henkelman, A. Arnaldsson, H. Jónsson, A fast and robust algorithm for Bader decomposition of charge density, Comput. Mater. Sci. 36 (2006) 354–360.
[43] R.S. Mulliken, Electronic population analysis on LCAO–MO molecular wave functions. I, J. Chem. Phys. 23 (1955) 1833–1840.
[44] M. Zhu, W. Song, P.M. Konze, T. Li, B. Gault, X. Chen, J. Shen, S. Lv, Z. Song, M. Wuttig, R. Dronskowski, Direct atomic insight into the role of dopants in phase-change materials, Nat. Commun. 10 (2019) 3525.
[45] C. Kittel, P. McEuen, P. McEuen, Introduction to Solid State Physics, Wiley, New York, 1996.